Journal of Sustainable Development of Energy, Water and Environment Systems

http://www.sdewes.org/jsdewes

Year 2025, Volume 13, Issue 4, 1130637

Original Research Article

Solar-Based Electric Vehicle Charging with Bidirectional Buck-Boost Converter and Proportional-Integral Control Algorithm

M.I.M. Mawardi[1], N.H.Nik Ali[*2], M.N. Hidayat[2], E. Abdullah[2], M. Umair[2], M.A.T Mat Yusof[2]

[1]Battery Energy Storage Technology Laboratory (BESTLab), College of Engineering, Universiti Teknologi MARA, Malaysia.
e-mail: muhammadizzulizz972@gmail.com

[2]School of Electrical Engineering, College of Engineering, Universiti Teknologi MARA, Malaysia.
e-mail: hakimiali@uitm.edu.my

Cite as: Bin Mohd Mawardi, M. I., Nik Ali, N. H., Hidayat, N. M., Abdullah, E., Umair, M., Mat Yusof, M. A. T., Solar-Based Electric Vehicle Charging with Bidirectional Buck-Boost Converter and Proportional-Integral Control Algorithm, J.sustain. dev. energy water environ. syst., 13(4), 1130637, 2025, DOI: https://doi.org/10.13044/j.sdewes.d13.0637

ABSTRACT

As electric vehicle adoption accelerates, the development of sustainable and efficient charging infrastructure is essential. This study presents a novel electric vehicle charging system that integrates solar photovoltaic energy with an energy storage system using a bidirectional buck-boost converter. The converter enables energy flow in both directions between the energy storage system and the electric vehicle, allowing flexible operation under varying energy availability. A control framework combining maximum power point tracking and proportional-integral control is implemented to regulate power flow and enhance system stability. MATLAB-based analysis evaluates system performance under different operational scenarios. Results show that the integration of an energy storage system reduces dependence on grid electricity while maintaining charging efficiency. The bidirectional buck-boost converter achieves high efficiency in both charging and discharging modes, enabling optimal energy utilization across solar, storage, and electric vehicle components. This work contributes to the advancement of smart and renewable-based electric vehicle charging infrastructure by improving energy flexibility, reliability, and sustainability.

KEYWORDS

Bidirectional converter, Electric vehicle, Energy storage system, Control algorithm, Solar system.

INTRODUCTION

Electric vehicles (EVs) are a type of vehicle that runs on electricity, as opposed to gasoline or diesel [1]. EVs are equipped with electric motors that are powered by rechargeable batteries [2], [3]. These vehicles are gaining popularity due to environmental concerns and lower operating costs [4], [5]. EVs produce no emissions, are more energy efficient than traditional gasoline vehicles and provide a quieter and smoother driving experience due to the immediate torque provided by the electric motor [6]. In addition, rising fossil fuel prices and government incentives for zero-emission transportation have further accelerated EV adoption across global markets [7], [8], [9]. With the advancement of technology, the driving range of EVs has also significantly increased, making them a practical and feasible option for many drivers [10].

* Corresponding author

As EVs become more widespread, one major challenge is how to efficiently charge them, especially in areas with limited access to the power grid. A possible solution to this problem is implementing an Energy Storage System (ESS) that utilizes solar energy to charge EVs [11], [12], [13], [14]. Several studies have explored solar-assisted EV charging architectures, especially in regions with high solar irradiance and unreliable grid supply. There are multiple options available for EV chargers, each with its own set of advantages and disadvantages. These options range from basic Level 1 chargers, which can be plugged into a standard household outlet, to fast Direct Current (DC) chargers that can charge up to 80% in just 30 minutes, to wireless chargers that use magnetic induction[15]. In this age of rapid technological advancement, the future of EV charging is promising, with new and improved charging solutions being developed regularly [16]. It suggests using an off-grid solar PV system to reduce installation costs, lower energy-related costs through local solar power generation and provide EV charging options in locations without sufficient grid infrastructure. This approach could offer significant benefits for both facility operators and EV owners.

The power supply to the EV can be Alternating Current (AC) or Direct Current (DC) type. AC-type power flow is not suitable for the EV charging station as it increases the charging time. The DC-type power flow reduces the charging time and increases the performance of the EVs [17]. Previous research has also focused on optimising charging schedules and power management to reduce strain on local grids and improve energy efficiency during peak demand periods [18], [19], [20]. **Table 1** provides information on the different types of Electric Vehicle Supply Equipment (EVSE) and corresponding power supply, charge power, and charging time for a 24 kWh battery [21].

The first type of EVSE mentioned is the AC charging station for residential use, also known as Level 1 (L1). It has a single-phase 120/230 VAC power supply with a current rating of 12 A to 16 A, which translates to an approximate charge power of 1.44 kW to 1.92 kW. With this charging station, it takes approximately 17 hours to charge a 24 kWh battery fully. The second type of EVSE mentioned is the AC charging station for commercial use, also known as Level (L2). It has a power supply of 208-240 VAC and 15 A to approximately 80 A single or three-phase, which translates to an approximate charge power of 3.1 kW to 19.2 kW. With this charging station, it takes approximately 8 hours to charge a 24-kWh battery fully. The third type of EVSE mentioned is the DC charging station, also known as the Level 3 (L3) fast charger. [22]. It has a power supply of 300 to 600 VDC and a maximum of 400 A, which can deliver a charge power from 120 kW up to 240 kW. With this charging station, it takes approximately 30 minutes to charge a 24 kWh battery to 80% capacity, which is significantly faster compared to AC charging stations. It is worth noting that the charging time can vary depending on factors such as the capacity of the battery, the state of charge (*SOC*) of the battery at the start of the charging process, and the charging speed of the specific EVSE being used. [23], [24].

Table 1. Charging station classification

EVSE Type	Power Supply	Charge Power	Charge Time
AC charging station: L1 residential	120/230 VAC and 12 A to 16 A (single phase)/320 VAC and 12	Approximately 1.44 kW to approximately 1.92 kW	Approximately 17 hours
AC charging station: L2 commercial	208-240 VAC and 15 A to approximately 80 A (single/split phase)	Approximately 3.1 kw to approximately 19.2 kW	Approximately 8 hours
DC charging station: L3 fast chargers	300 to 600 VDC and (Max 500 A) (poly phase)	From 120 kW up to 240 kW	Approximately 30 minutes

The bidirectional DC-DC converter (BDC) is attracting growing interest due to its potential applications in electric vehicle chargers, solid-state transformers, and energy storage systems, enabling both grid-to-vehicle (G2V) and vehicle-to-grid (V2G) operations [25]. Its key advantages include efficient soft-switching operation and a broad voltage conversion range [24]. Battery electric vehicles (BEVs), which are charged in the parking lot, arrive and depart during a year-long simulation of electricity production from the photovoltaic array [17]. A simulation was conducted to analyse the parking lot's operation over a year to evaluate the efficacy of EV charging using an off-grid solar PV system [26], [27]. Based on the simulation results, several strategies were proposed to improve the charging capability of the EV fleet, and a comparison was made among them [28]. The system was designed for grid-connected EV charging in a workplace parking lot in the Netherlands [29]. They explored the possibility of increasing the capacity of stationary batteries to reduce the reliance on the grid for providing sufficient charging to plugged-in vehicles. However, even with extremely large battery packs per carport, equivalent to the capacity of EV batteries themselves, it was found that the complete elimination of grid reliance for adequate charging was not achievable [28]. Similarly, researchers have studied hybrid systems integrating renewable energy, ESS, and demand response strategies to manage peak load and ensure energy reliability.

Although many EV charging systems incorporate solar energy or energy storage, they often do not provide flexible power management capable of handling renewable variability and dynamic load conditions. Moreover, conventional unidirectional or isolated converter systems are limited in supporting bidirectional energy flow, reducing their effectiveness in V2G or energy optimisation scenarios. [30]. This article presents a novel research study aimed at addressing these gaps by revolutionising the EV charging process through the incorporation of an ESS using a Buck-Boost DC-DC bidirectional converter with a control algorithm. [31]. The bidirectional converter enables the ESS to charge the EV and discharge it back to the ESS for energy storage. The study explores the potential of an off-grid solar photovoltaic system combined with an ESS, proposing an environmentally sustainable and reliable alternative to traditional unidirectional charging methods. This solution seeks to significantly reduce reliance on the power grid, offering a viable option where grid access is limited.

METHODS

This section outlines the methods for designing a Buck-Boost bidirectional converter and integration system. It covers the research system design, solar system integration, energy storage system integration, Electric vehicle charger model, Electric Vehicle integration, Buck-Boost bidirectional converter, operation mode, controller for bidirectional converter, controller tuning, and system integration.

Overall System Design

Figure 1 presents the DC bus, which serves as the central link, enabling efficient energy flow between components. The solar PV system connects to the DC bus through a Maximum Power Point Tracking (MPPT) DC-DC converter to ensure maximum energy harvesting. The ESS is interfaced via a bidirectional DC-DC converter, allowing it to store surplus solar energy and discharge power when needed to support EV charging or supplement grid demand [22]. The EV block includes a battery and electric motor connected through a DC-AC inverter, with the EV battery charged or discharged through the same bidirectional converter to support functions like V2G [16]. On the grid side, a bidirectional AC-DC converter enables energy exchange with a 400 V, 50 Hz three-phase AC grid. Based on the Nissan Leaf EV specifications, each charger is rated for 400 V DC and 40 kW. The integration of solar and ESS with smart bidirectional control enhances energy flexibility, reduces reliance on the grid, and ensures stable power supply to meet dynamic EV charging demands.[23], [24], [27].

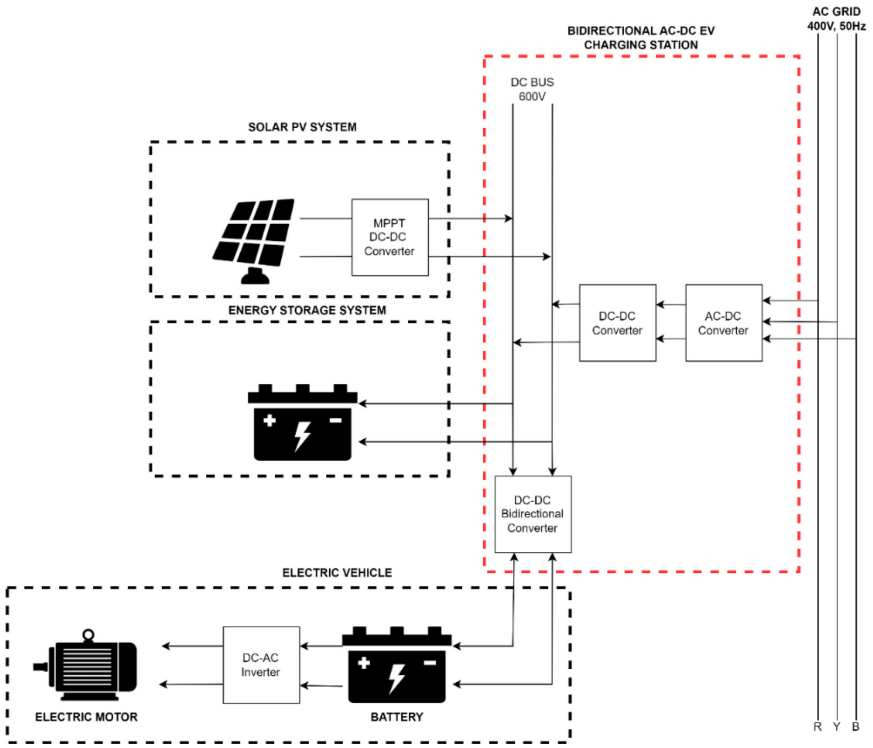

Figure 1. Layout diagram of proposed bidirectional AC-DC EV Charging Station

Solar System Integration

Figure 2 presents the design of a solar system with a PV panel and an MPPT.In the proposed solar PV system, a PID-based MPPT controller is implemented in conjunction with a boost converter. The PID controller continuously monitors the error between the PV panel voltage and the reference voltage corresponding to the MPPT. By adjusting the duty cycle of the boost converter, the PID controller ensures the PV operates at its optimal point, thereby maximising power extraction. The boost converter steps up the PV output voltage to match the required level for efficient ESS charging. This configuration improves energy harvesting efficiency while maintaining stable system performance under varying irradiance and temperature conditions **[32]**.

In this setup. the solar system was set up with 15 panels in series and 8 parallel connections that produce a maximum power of 46 kW with voltage and current 607.5 V and 75.12 A at higher irradiance, The configuration optimization process involved varying irradiance from 500 W/m² to 1000 W/m², temperature from 10 °C to 50 °C, and validating the series/parallel arrangement to ensure voltage and current compatibility while minimizing mismatch losses. This means that to achieve optimal performance and maximise energy production, solar energy systems must be designed and installed in locations where they receive sufficient sunlight exposure **[33]**.

Moreover, variations in the amount of solar irradiance received throughout the day and across different seasons must be considered to ensure that the system can meet the energy demands of the charging infrastructure. **Table 2** presents solar specifications for the single panel, which includes a maximum power output of 380 W, total cells of 72, a corresponding maximum voltage of 40.5 V, and a maximum current of 9.39 A. Additionally, **Table 2** provides information on the open circuit voltage and short circuit current, which are 48.9 V and 9.75 A, respectively. The temperature coefficients of open circuit voltage and short circuit voltage are also presented, with values of -0.326 %/°C and 0.055005 %/°C, respectively. The objective function was to maximise total electrical power delivered to the ESS while keeping voltage and current within safe operating limits for the downstream converter and storage system. The PID-based MPPT approach was selected for its fast dynamic response, ease of

implementation, and stable performance under fluctuating irradiance and temperature, and simulation results confirmed that this configuration improved overall energy harvesting efficiency and ensured consistent charging capability for the intended EV charging infrastructure..

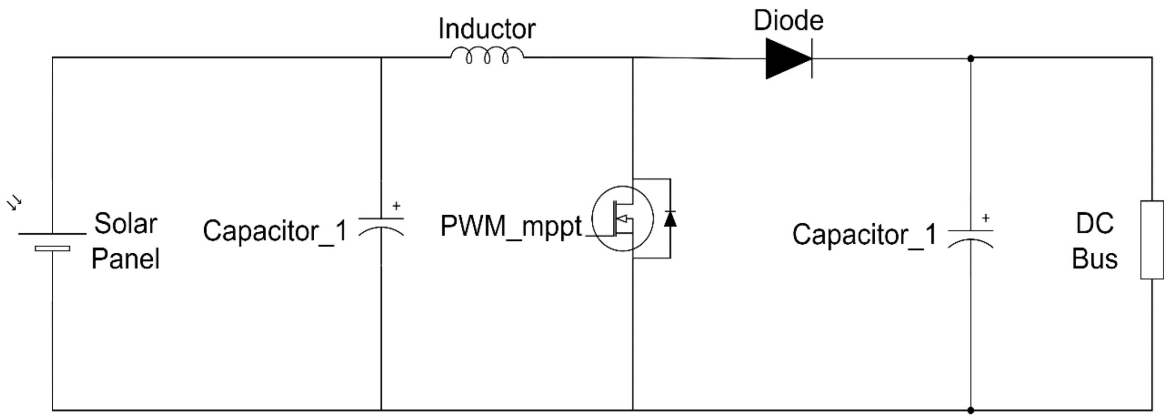

Figure 2. Boost Converter with MPPT control

Table 2. Solar specifications for a single panel

Specifications	Value
Maximum Power (P_{max}) per module	780 W
Cell per module	72 N_{cell}
Maximum Voltage Power (V_{mp})	40.5 V
Maximum Current Power (I_{mp})	9.39 A
Open Circuit Voltage (V_{oc})	48.9 V
Short Circuit Voltage (I_{sc})	9.75 A
Temperature Coefficient of V_{oc}	-0.326%/°C
Temperature coefficient of I_{sc}	0.055005%/°C

Energy Storage System Integration

Table 3 represents the battery for the ESS specification. A battery model was developed using a lithium-ion type battery to integrate with the ESS. The model consists of one bank battery with 600 VDC 100 Ah connected in series.

Table 3. Energy storage system specifications

Specifications	Value
Nominal Voltage	600 V
Rated Capacity	100 Ah
Maximum Voltage	698 V
Cut-off Voltage	450 V
Nominal Discharge Current	22 A

The battery model includes parameters such as capacity, efficiency, and charging or discharging rates. *SOC* represents how much energy is currently stored in the battery relative

to its full capacity. *SOC* expression is shown in eq. (1). In ESS, there are two processes, charging and discharging. The expression of charging and discharging is shown in eq. (2) and eq. (3):

$$SOC(\%) = \frac{C_r\ (\text{Ah})}{C_t\ (\text{Ah})} \tag{1}$$

where *SOC* (%) is the state of charge, C_r is the remaining capacity and C_t is the total capacity,

$$Charging\ Time(t) = \frac{C_b\ (\text{Ah})}{I_c\ (\text{A})} \tag{2}$$

where C_b is the battery capacity and I_c is the charging current,

$$Discharging\ Time(t) = \frac{C_b\ (\text{Ah})}{I_d\ (\text{Ah})} \tag{3}$$

where I_d is the discharging current.

Electric Vehicle Charger Model

An EV charger model was developed to receive energy from the three-phase incoming supply and the ESS to charge EVs [34]. The model consists of a one-unit 40 kW AC/DC charger model. The overall circuit of the AC/DC Charger is shown in **Figure 3**, which consists of three main components, the connection control and AC/DC converter, and the DC/DC converter. The charger model includes parameters such as the charging rate and voltage level. This system is designed by using an AC/DC EV charger, but another DC/DC converter was added to the existing AC/DC charger shown in **Figure 4** to allow bidirectional charging and discharging between the EV charger and ESS. This converter will help smooth the operation of the ESS to AC-DC EV charger. Besides, AC input from incoming, ESS can also act as an incoming supply that supports the solar system to deliver power to existing AC/DC chargers.

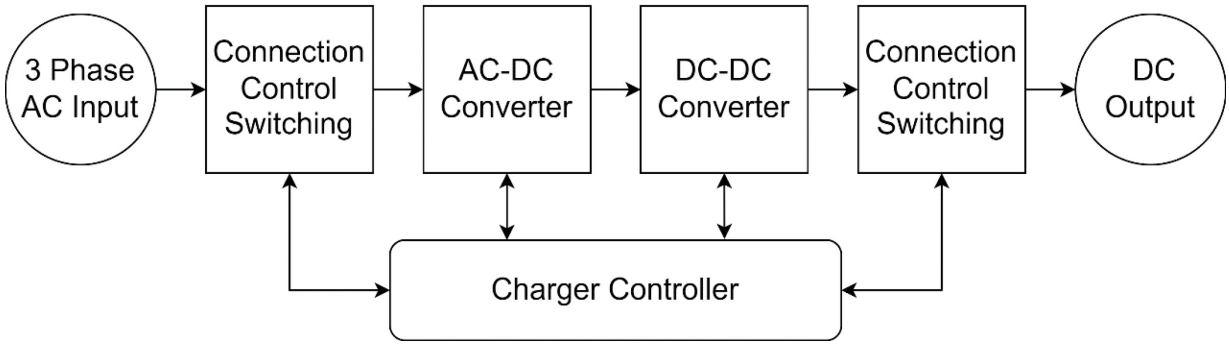

Figure 3. An overall diagram of the AC/DC Charger

Electric Vehicle Integration

An EV model was developed to receive energy from the AC/DC Charger. **Table 4** shows EV battery specifications. EV battery capacity is 20 kWh and consists of 400 V and 50 Ah using Lithium-ion type. The selection of EV battery specifications referred to existing EV battery specifications in the current industry model. Onboard EVs can control power flow inside of EVs with protection.

Table 4. Electric vehicle specifications

Specifications	Value
Nominal Voltage	400 V
Rated Capacity	50 Ah
Maximum Voltage	466 V
Cut-off Voltage	300 V
Nominal Discharge Current	22 A

Buck-Boost Bidirectional Converter Model

To control the charging and discharging of ESS and EV batteries, a buck-boost bidirectional DC-DC converter was introduced [24], as shown in **Figure 4**, to ensure the flow of current can occur in both directions, with or without the presence of an EV, while maintaining current stability using the PI controller algorithm. For buck mode (ESS to EV), the current is flowing when S_1 is ON, S_2 is OFF and both the diodes D_1 and D_2 are reverse biased. The energy stored in the inductor will discharge in a negative slope. Diode D_2 is ON, D_1 is reverse biased and S_1 and S_2 are OFF. During regenerative braking, this mode of operation is employed to charge the EV battery. For boost mode (EV to ESS), S_2 is ON and S_1 is OFF, the inductor charges and the current will increase linearly. Diode D_1 is ON, S_1 and S_2 are OFF and diode D_2 is reverse biased. The energy accumulated in the inductor will start discharging through diode D_1. In this mode, the energy from the source and inductor will be fed to the load, thus there will be a step up in voltage level.

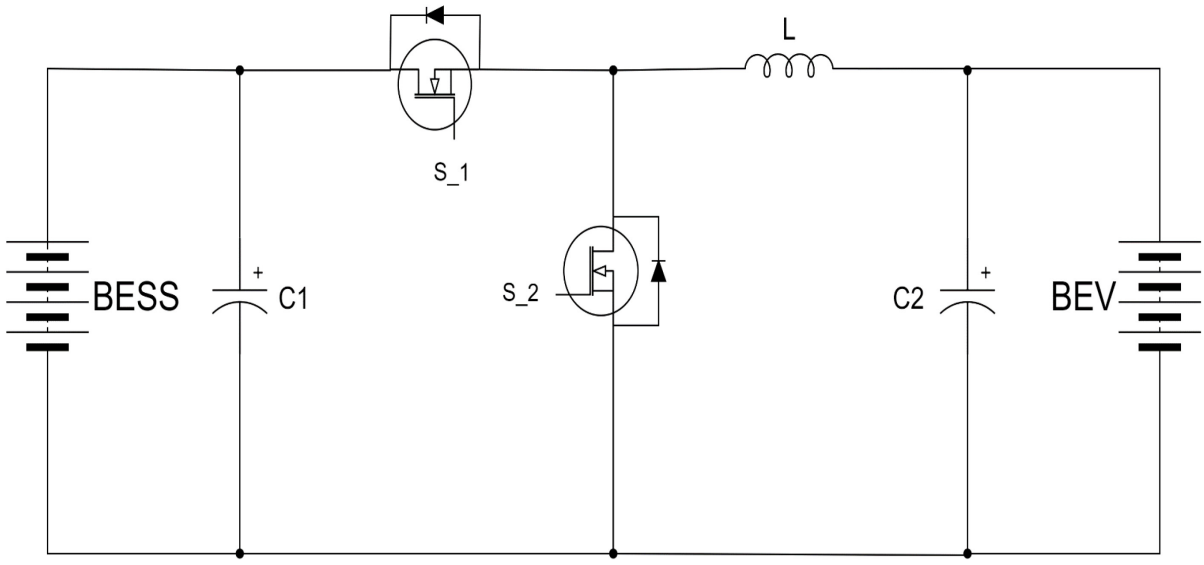

Figure 4. Buck-Boost bidirectional DC-DC converter

The equations describe the relationship between input and output power. Eq. (4) shows that input power P_{in} is the product of input voltage V_{in} and input current I_{in}. Eq. (5) defines output power P_{out} as the product of output voltage V_{out} and output current I_{out}. Eq. (6) expresses output power P_{out} in terms of output voltage squared divided V_{out}^2 by load resistance R:

$$P_{in} = V_{in} I_{in} \tag{4}$$

$$P_{out} = V_{out} I_{out} \tag{5}$$

$$P_{\text{out}} = \frac{{V_{\text{out}}}^2}{R} \tag{6}$$

Eq. (7) defines the duty cycle D of a converter as the ratio of the absolute value of the output voltage $|V_{\text{out}}|$ to the sum of the input voltage V_{in} and the absolute output voltage. The duty cycle D determines the proportion of time the switch is on during each cycle, affecting the overall voltage regulation and power transfer efficiency of the converter:

$$D = \frac{|V_{\text{out}}|}{V_{\text{in}} + |V_{\text{out}}|} \tag{7}$$

Eq. (8) represents the inductor current I_{L} in a converter, calculated as the product of the input voltage V_{in} and the duty cycle D, divided by the resistance R and the square $(1 - D)$. This formula helps determine the current flowing through the inductor, which is critical for analysing the converter's operation and performance, particularly in managing energy storage and power delivery:

$$I_{\text{L}} = \frac{V_{\text{i}} D}{R(1 - D)^2} \tag{8}$$

Eq. (9) and eq. (10) describe the maximum I_{max} and minimum inductor currents I_{min} in a converter, where V_{in} is the input voltage, D in duty cycle, R is the load resistance, T is switching time, and L is an inductor:

$$I_{\text{max}} = \ = \frac{V_{\text{in}} D}{R(1 - D)^2} + \frac{V_{\text{in}} DT}{2L} \tag{9}$$

$$I_{\text{min}} = \ = \frac{V_{\text{in}} D}{R(1 - D)^2} - \frac{V_{\text{in}} DT}{2L} \tag{10}$$

Eq. (11) calculates the minimum inductance L_{min} necessary for the proper operation of a converter, given $\frac{(1-D)^2 R}{2f_{\text{s}}}$ where D is the duty cycle, R is the resistance, and f_{s} is the switching frequency. This equation helps ensure that the inductor is sized correctly to maintain circuit stability and minimize current ripple:

$$L_{\text{min}} = \frac{(1 - D)^2 R}{2f_{\text{s}}} \tag{11}$$

Eq. (12) calculates the capacitance C needed in a converter circuit, given by $\frac{D}{Rrf_{\text{s}}}$) where D is the duty cycle, R is the load resistance, r is a ripple voltage, and f_{s} is the switching frequency. This formula helps determine the appropriate capacitor value to ensure stable voltage regulation and minimize voltage ripple in the circuit:

$$C = \frac{D}{Rrf_{\text{s}}} \tag{12}$$

Eq. (13) expresses the efficiency n of the Buck-Boost converter to identify the performance of the converter as the ratio of the output power P_{out} to input power P_{in}. This ratio measures how efficient the system converts the input power into output, with a higher ratio indicating better performance and lower power losses:

$$n = \frac{P_{\text{out}}}{P_{\text{in}}} \times 100 \quad (13)$$

Operation Mode

This operation mode is crucial for controlling the charging ESS from the solar system for mode 1 and bidirectional flow in Mode 2 and Mode 3, which represent EV charging and discharging, respectively.

a) Mode 1- Charging ESS using Solar System Integration

Mode 1 operation, the charging of the ESS occurs gradually over time. This gradual charging process ensures that the ESS is consistently topped up with energy, maximizing its storage capacity for future use. By charging the ESS during periods of low demand, the system ensures that renewable energy generated by the solar panels is effectively harnessed and stored for times when it is needed

b) Mode 2- Charging EV using ESS Integration

Mode 2 operation involves charging the EV battery using the ESS through a bidirectional converter operating in buck mode. This mode is particularly valuable during grid outages or peak load conditions, providing a backup power solution by stepping down the 600 V from the ESS to the 400 V required by the EV battery. This ensures continuous availability of power for EV charging, enhancing the system's resilience and reliability.

c) Mode 3- Discharging EV to ESS Integration

Mode 3 operation enables the discharge of energy from the EV battery back to the ESS, functioning in boost mode. This mode is critical when the ESS needs to be recharged or when the grid is not supplying adequate power. By stepping up the 400 V from the EV to the 600 V needed by the ESS, this mode allows for effective energy transfer, optimizing energy use and maintaining balance in the system during varying power demands.

Controller for Bidirectional Converter

This section presents the charging and discharging control algorithms for the bidirectional converter. A PI-based PWM generator is implemented for controlling the bidirectional battery charger circuit using a Buck-Boost converter. The comparator compares the reference current and actual current, the output of the comparator generator error signal.

Figure 5 shows the operation switch of the BDC to change between two modes: The bidirectional operation will set '1' for charging EV to represent mode 2 and '0' for discharging EV to represent mode 3. If *BDC_sw* set into 1, the operation will select Ib_ref_charge as battery current reference, while *BDC_sw* set to 0, the operation will select $Ib\_ref\_discharge$ as battery current reference and allow operation mode of bidirectional.

During the mode 2 operation in **Figure 6**, the EV battery charges, while the ESS battery discharges simultaneously. The converter's input voltage is the DC-link voltage $VbatESS$ generated by the ESS battery, and the output of the converter is the battery voltage $VbatEV$. Initially, the DC-link voltage $VbatESS$ energizes both the inductor and the EV battery. Once the inductor is fully energized, the battery is charged solely by the energy stored in the inductor. The algorithm compares the measured $VbatEV$ with the desired EV battery voltage of 466 V. A PI voltage controller then minimizes and eliminates the error to ensure they are equal until the EV battery reaches 100% *SOC*. In this system, the output signal of the voltage controller is defined as the reference current charging signal Ib_ref_charge, which is set in the PI controller.

In the mode 3 operation, the control algorithm in **Figure 7** regulates the discharging of the EV battery and the charging of the ESS battery simultaneously. The converter's input voltage is the DC-link voltage $VbatEV$ generated by the EV battery, and the output of the converter is the battery voltage $VbatESS$. Initially, the DC-link voltage $VbatEV$ energizes both the inductor and the ESS battery. Once the inductor is fully energized, the ESS battery is charged solely by the energy stored in the inductor. The algorithm compares the measured $VbatESS$ with the desired ESS battery voltage 698 V. A PI voltage controller then minimizes and eliminates the error to ensure they are equal until the ESS battery reaches 100% SOC. In this system, the output signal of the voltage controller is defined as the reference current charging signal $Ib\_ref\_discharge$, which is set in the PI controller.

The algorithm compares the measured battery current $IbatEV$ and the reference current $Ibat\_ref$ from the operation of the BDC. A PI current controller then minimizes and eliminates the error to ensure $IbatEV$ and the reference current $Ibat\_ref$ is equally shown in **Figure 8**. The converter can operate in constant current (CC) mode during the initial charging phase and constant voltage (CV) mode as the battery approaches full charge. This CC and CV charging strategy ensures safe and efficient charging, preventing overcharging and extending battery life **[35]**. Lastly, the control algorithm regulates the charging or discharging process by controlling the two MOSFET switches (S_P1 and S_N1). **Figure 9** shows the typical waveform of the Buck-Boost converter for the switching strategy.

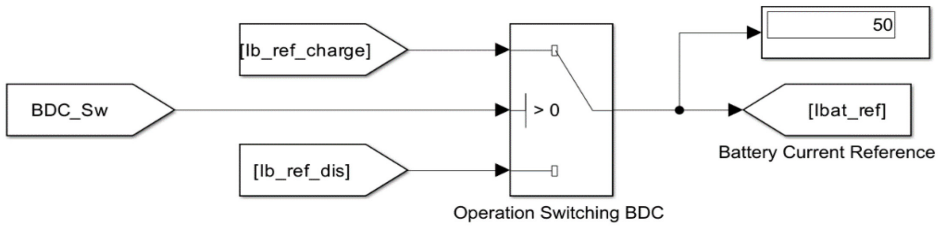

Figure 5. Operation Switching of Bidirectional Flow

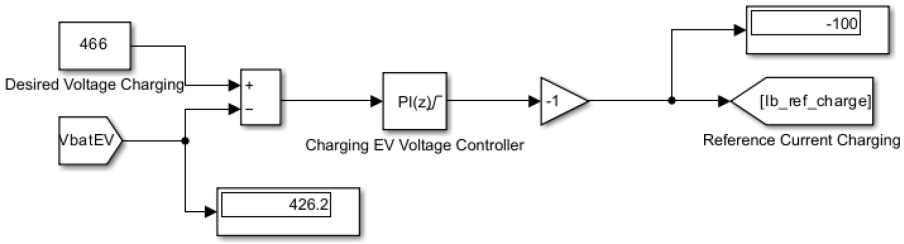

Figure 6. Reference Current for Charging EV Operation

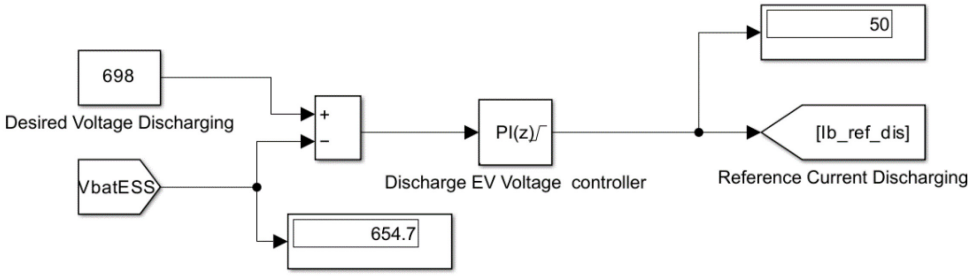

Figure 7. Reference Current for Discharging EV Operation

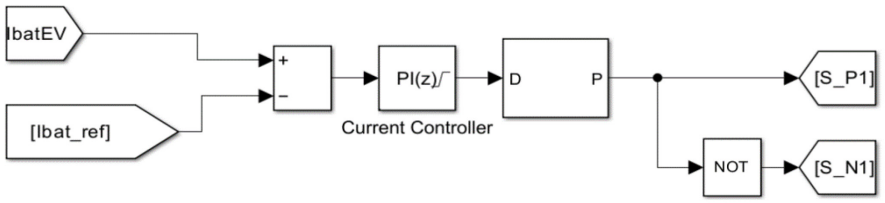

Figure 8. PI Controller for PWM Control

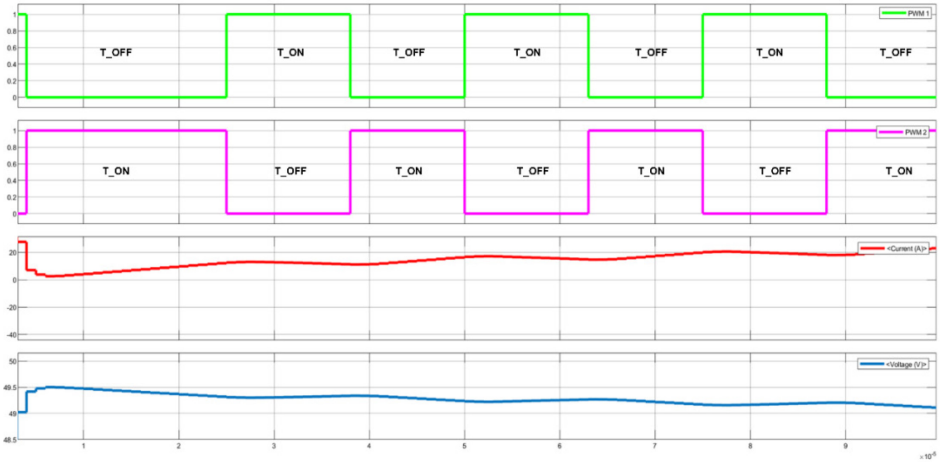

Figure 9. Typical Waveform of the Buck-Boost Converter

Controller Tuning

Eq. (14) expresses the PI controller in a transfer function form PI:

$$PI(s) = K_{\mathrm{P}} + \frac{K_{\mathrm{I}}}{s} \tag{14}$$

The proportional gain K_{P} controls the error magnitude by applying a correction proportional to the error. $(\frac{K_{\mathrm{I}}}{s})$ is integral gain to eliminate steady-state error by summing up the accumulated error over time. In this study, K_P set to 0.25 and K_{I} set to 50, and the PI controller parameters were tuned using a combination of the Ziegler–Nichols closed-loop method and simulation-based iterative refinement to ensure accurate current tracking and system stability in both EV charging and discharging modes. The PI controller parameters were tuned using a combination of simulation-based iterative adjustment and performance-based criteria to ensure accurate current tracking and system stability in both EV charging and discharging modes. Initially, a step-response test was conducted in MATLAB/Simulink to evaluate the system dynamics of the bidirectional converter and battery charging circuit.

Figure 10 demonstrates that the battery current adjusts to match the reference battery current using a tuned PI controller, proving its functionality in regulating the charging current. A comparator measures the difference between the reference current (desired current) and the actual current (measured current). The output of the comparator, the error signal, indicates the deviation of the actual current from the reference current. This error signal is then fed into the PI controller for further processing and produce bidirectional flow by charging EV and discharging EV mode operation through bidirectional converter. For example, when the reference battery current is set to 100 A at PI saturation, the actual battery current will also be 100 A and it will run into mode 2 operation.

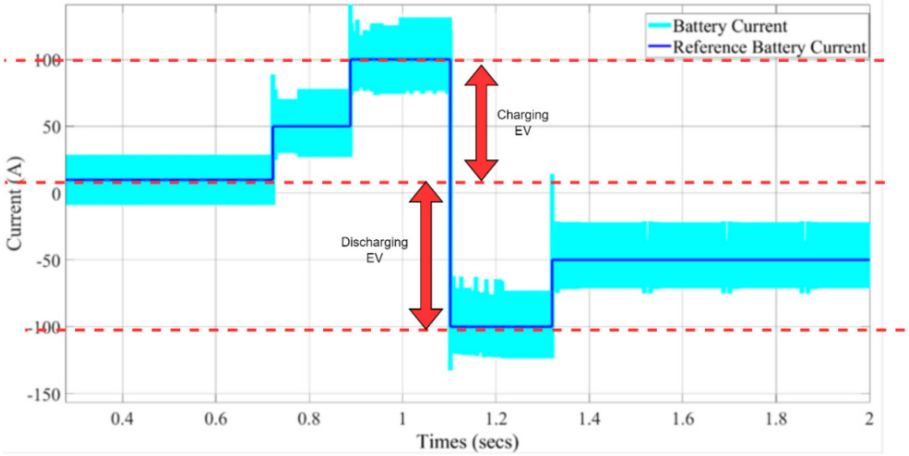

Figure 10. Tuning PI Controller

System Integration

Figure 11 illustrates a simulation configuration and integration of all systems. It is apparent that solar models, ESS battery models, electric vehicle charger models, and EVs were combined and integrated into a comprehensive single-system model. This approach enabled the evaluation of the system's overall efficiency and effectiveness, considering the interdependent functions and interactions of the solar panels, ESS battery storage, and EV charging components. The integrated system model allowed for a more accurate representation of the system's behavior, enabling a better understanding of the various factors that impact the performance of the renewable energy-powered EV charging system. The proposed system is inherently scalable due to its modular architecture and the use of a bidirectional buck-boost DC-DC converter, which supports flexible voltage and power control. When scaled to accommodate multiple EVs or a larger ESS, the converter and control algorithms can be adapted to manage increased power flow and dynamic load balancing. For multiple EVs, additional converter modules can be integrated in parallel, each with independent control, allowing simultaneous charging or discharging while maintaining system stability. For larger ESS capacity, the system can be scaled by adjusting the converter's power rating and storage management algorithms to ensure optimal energy utilization without overloading the PV source or grid interface. However, system coordination and communication between modules would become increasingly critical, requiring more advanced energy management strategies and possibly centralized or hierarchical control.

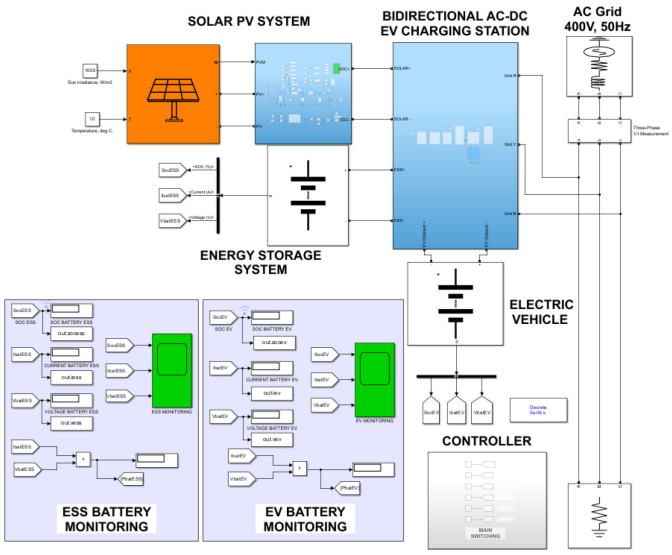

Figure 11. Simulation Configuration and Integration of All Systems

RESULT AND DISCUSSION

For the simulation study, 3 modes of ESS requirements are investigated. In Mode 1, Charging ESS using Solar system Integration, and in Mode 2, Charging EV using ESS Integration. Lastly, Mode 3 Discharging EV to ESS Integration. For Mode 2 and Mode 3, the test is conducted throuh Buck-Boost bidirectional converter.

Mode 1 – Charging Energy Storage System using Solar System Integration

Figure 12 illustrates that the PV output power increases proportionally with the rise in solar irradiance from 200 to 1000 W/m² with fix temperature at 10 °C. The voltage across the system remains relatively stable, ranging from approximately 623.11 V to 623.78 V, while the current increases from 12.4 A to 70 A in response to the increasing irradiance. This results in a corresponding power increase from around 7.7 kW to 43 kW. These results confirm the expected linear relationship between irradiance and power output in a photovoltaic system under stable temperature and voltage conditions. The best performance scenario occurs at an irradiance level of 1000 W/m², where the system achieves maximum power output and charging efficiency. This validates the design's capability to adapt to varying solar conditions while maintaining stable and efficient energy conversion, making it highly suitable for integration into solar-powered EV charging systems.

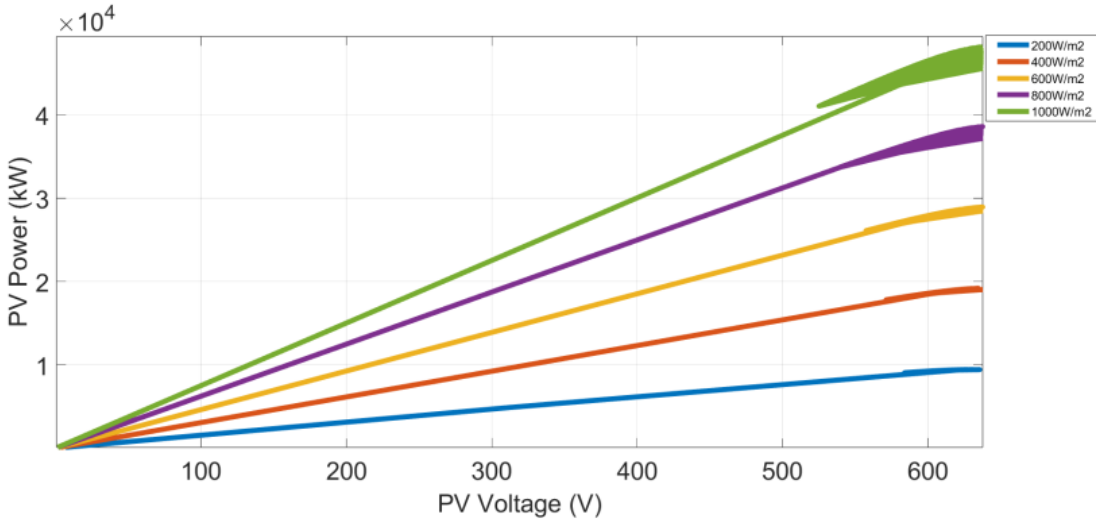

Figure 12. Relationship between solar Irradiance with Output power and voltage

Figure 13 illustrates the impact of temperature variations on PV output power at a constant solar irradiance of 1000 W/m². The graph shows a clear trend where lower temperatures result in higher power output, while increasing temperatures lead to a gradual reduction in PV performance. Specifically, at 10 °C, the system delivers the highest power output, approaching approximately 43 kW, whereas at 50 °C, the output power is slightly reduced due to the negative temperature coefficient of PV modules. This behavior is consistent with the physical characteristics of silicon-based solar cells, where higher temperatures tend to decrease voltage and, consequently, overall power output. Despite these temperature-induced variations, the system demonstrates reliable performance across the tested range (10 °C to 50 °C), indicating its robustness in maintaining stable charging conditions for the energy storage system. These results confirm that while temperature has a measurable effect on PV efficiency, the integrated system remains functional and efficient under diverse thermal conditions.

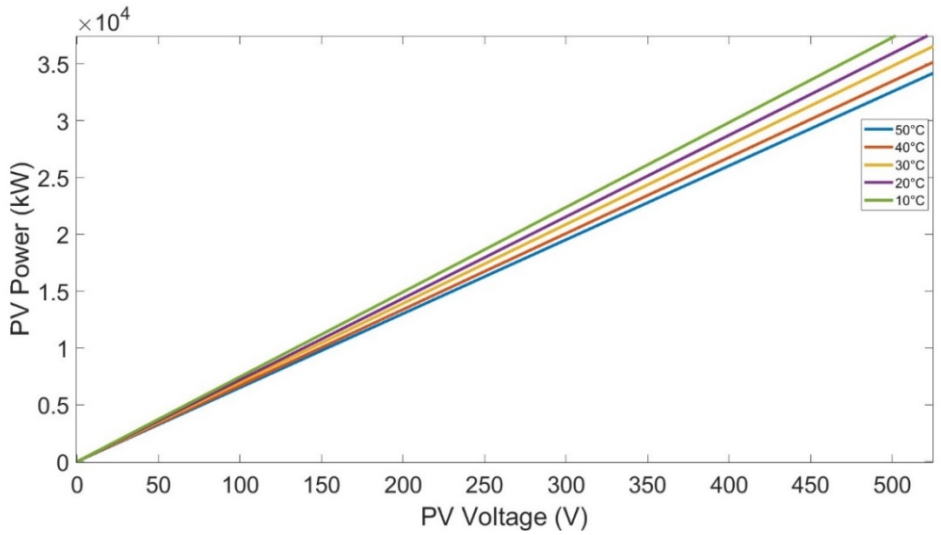

Figure 13. Impact of Solar Temperature on Output Power

The battery of ESS involves three parameters such as *SOC*, voltage, and current. **Figure 14** presents the *SOC*, current, and voltage of ESS waveforms during battery charging from solar. The effect of solar irradiance and temperature will change the output power of solar to charge ESS. The battery *SOC* increases with the maximum current provided by solar panels 1000 W/m² at 10 °C in **Figure 14a**. By using MPPT that consists of a boost DC-DC converter it will increase voltage from 300 V from solar panel to 640 V to charge ESS. This converter helps to minimize the use of quantity solar panels but can provide a high output voltage of ESS. However, since the maximum voltage and current provided by this MPPT are 657.58 V and 76.71 A shown in **Figure 14b** and **Figure 14c**, it takes longer times to increase the battery voltage and capacity of ESS 600 V and 100 Ah. From the calculation, the ESS will fully charge around 1.20 hours with maximum irradiance and suitable temperature. In conclusion, optimal efficiency in solar panels necessitates adherence to specific ranges of solar irradiance and temperature values. The defined ideal conditions, by standard testing conditions (STC), encompass a solar irradiance level of 1000 W/m² and a temperature of 10 °C. Elevated solar irradiance levels positively influence power output, while the peak efficiency of solar panels is observed at lower temperatures. The rise in temperature triggers efficiency reduction, attributed to the temperature coefficient effects expounded upon earlier.

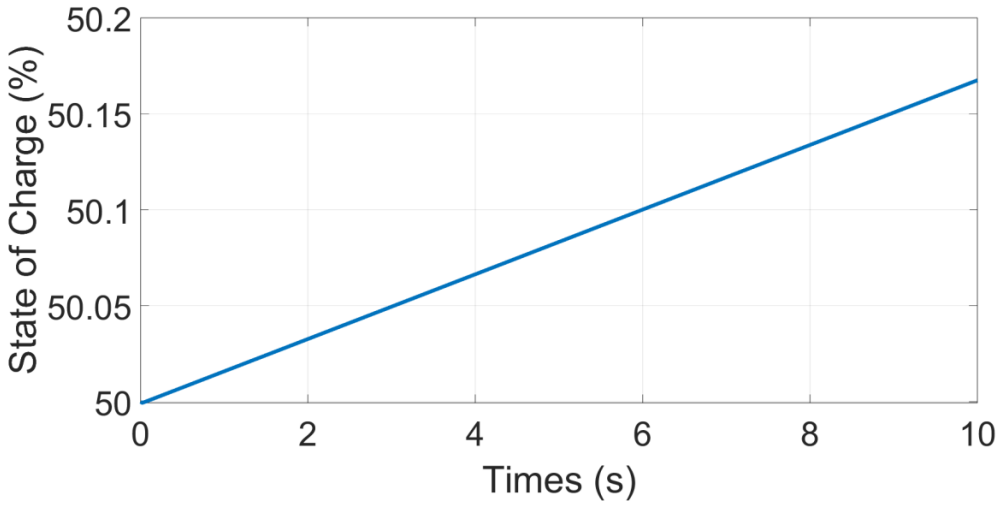

(a)

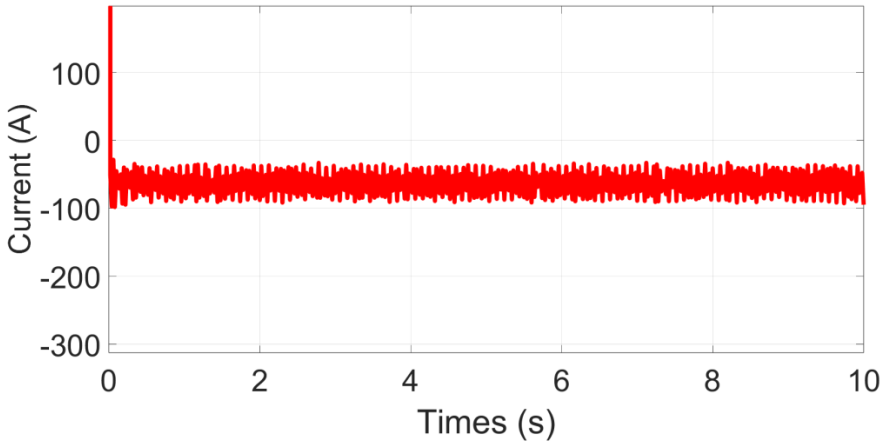

(b)

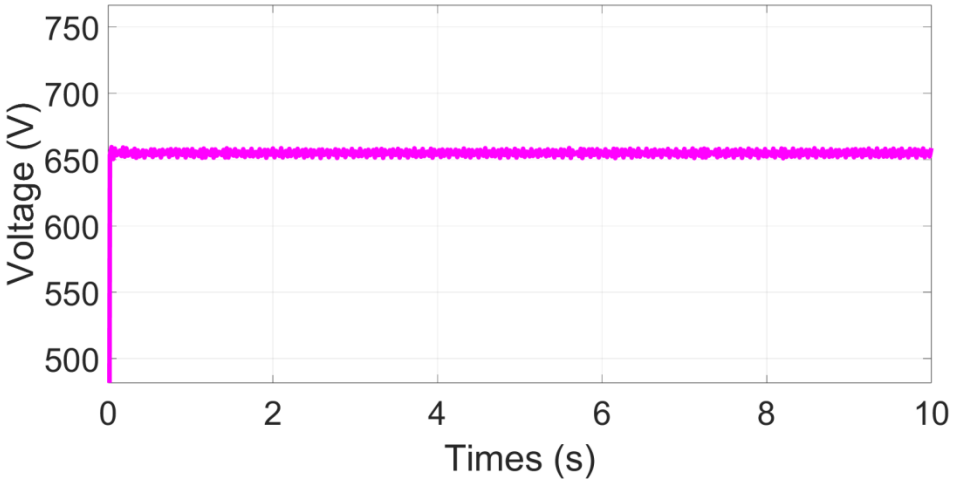

(c)

Figure 14. Charging ESS from solar (Mode 1): SOC (a); Current (b), and Voltage (c)

Mode 2 – Charging Electric Vehicle using Energy Storage System Integration

Figure 15 demonstrates the *SOC* dynamics. The *SOC* of the ESS gradually decreases from 50% to approximately 49.9%, indicating discharging over 10 seconds. Simultaneously, the *SOC* of the EV increases from 50% to about 50.25%, representing the transfer of energy from the ESS to the EV battery. The ESS experiences a 0.1% drop in *SOC*, while the EV gains 0.25% *SOC* over 10 seconds. Figure 16 illustrates the current behavior during the energy transfer. The ESS current is positive, indicating discharging, with fluctuations around 40 A due to losses at the high voltage side. On the other hand, the EV current is negative, indicating charging, with fluctuations around 50 A. These variations in current are due to the operation of a PI controller, ensuring stable energy transfer. Figure 17 shows the voltage profiles of both the ESS and the EV. The ESS maintains a voltage of around 600 V, while the EV voltage stabilizes around 400 V. These steady voltage levels suggest a smooth and well-regulated energy transfer between the ESS and the EV with buck operation. The bidirectional DC-DC converter operated in buck mode, reducing voltage from 600 V to 400 V while maintaining a peak efficiency of 95.3%. The power transfer rate was approximately 20 kW. Overall, the system demonstrates effective energy transfer with stable voltage levels and controlled current variations, supporting balanced operation during the charging process for mode 1 of Buck-Boost converter.

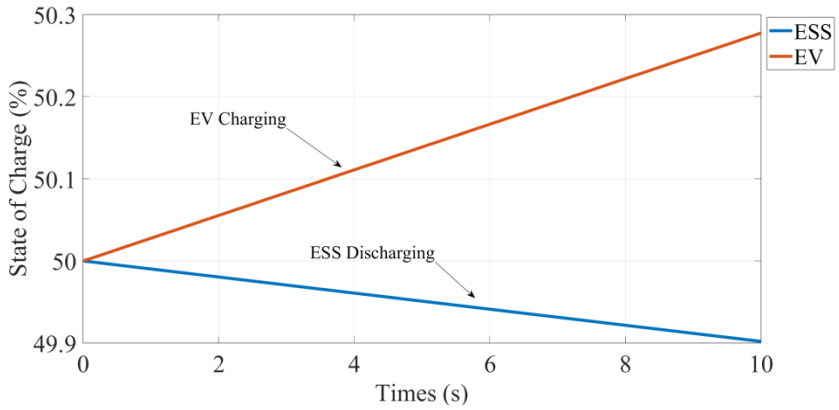

Figure 15. Battery SOC vs Times (Mode 2)

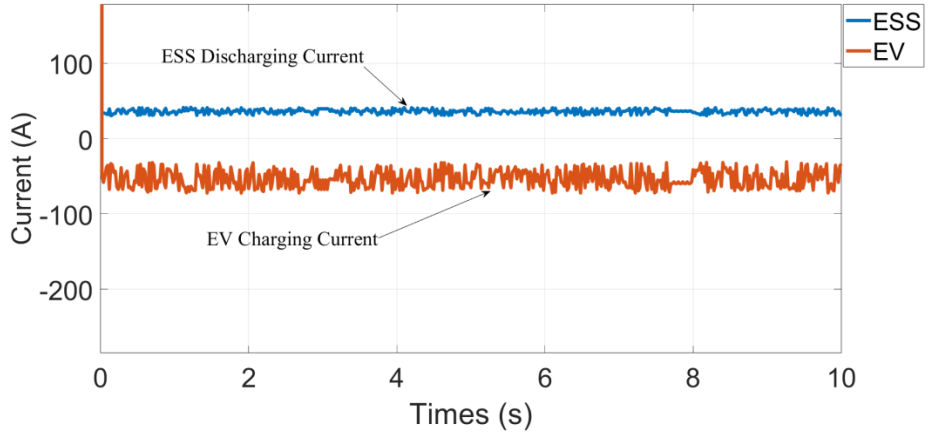

Figure 16. Battery Current vs Times (Mode 2)

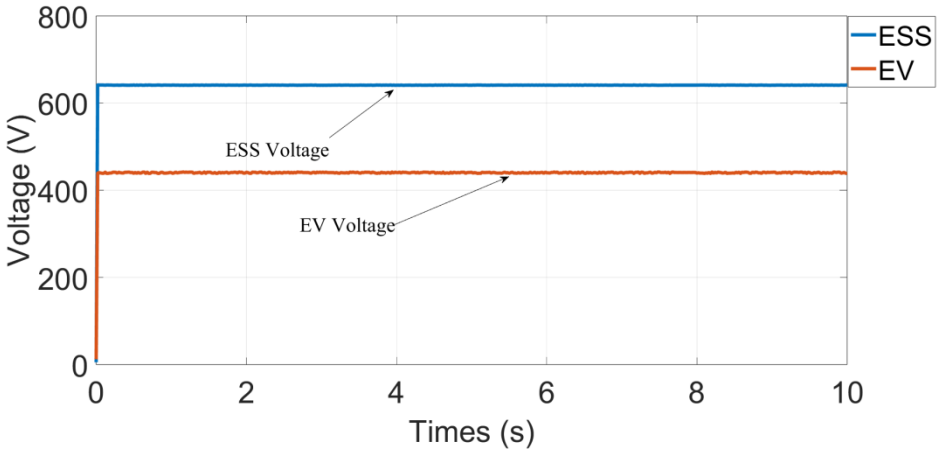

Figure 17. Battery Voltage vs Times (Mode 2)

Mode 3 – Discharging Electric Vehicle to Energy Storage System Integration

Figure 18 shows the *SOC* dynamics. The *SOC* of the ESS increases gradually from 50% to approximately 50.18%, indicating charging over 10 seconds. Simultaneously, the *SOC* of the EV decreases from 50% to about 49.5%, representing the energy transfer from the EV to the ESS. Over 10 seconds, the ESS gains 0.18% *SOC*, while the EV loses 0.5%, indicating a steady energy flow between the two systems. Figure 19 illustrates the current behavior during this process. The ESS current is negative, indicating charging, and fluctuates around 50 A. Conversely, the EV current is positive, signifying discharging, and fluctuates around 100 A. These fluctuations in

current are likely the result of a PI controller's operation to maintain balance and regulate the transfer of energy efficiently. **Figure 20** presents the voltage profiles for both the ESS and the EV. The ESS maintains a voltage of around 600 V, while the EV stabilizes at approximately 400 V, with both systems displaying minimal voltage variation throughout the 10 seconds with boost operation. The bidirectional DC-DC converter operated in boost mode, stepping up the voltage from 400 V to 600 V with a peak efficiency of 94.8%. The power transfer rate during discharging was measured at 22 kW. This stable voltage profile reflects a well-regulated energy transfer process, ensuring efficient charging and discharging operations between the EV and the ESS.

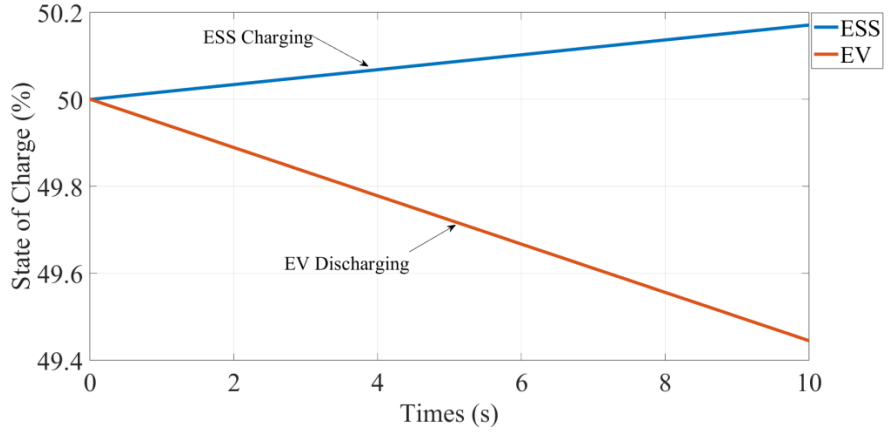

Figure 18. Battery Voltage vs Times (Mode 3)

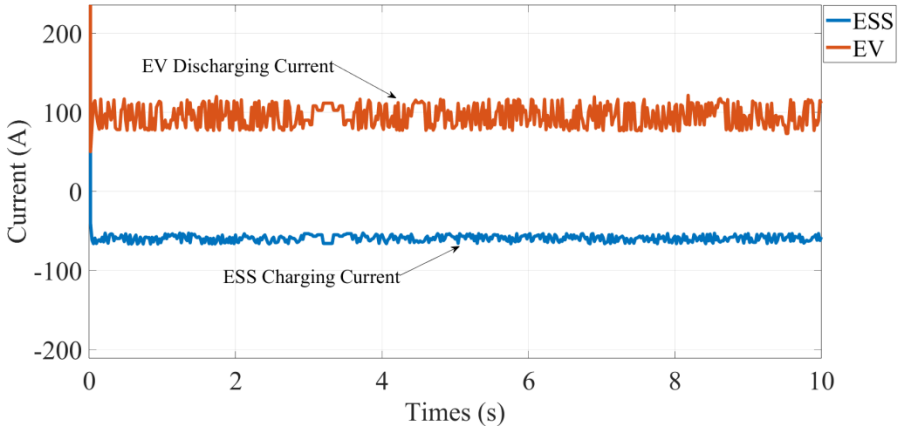

Figure 19. Battery Current vs Times (Mode 3)

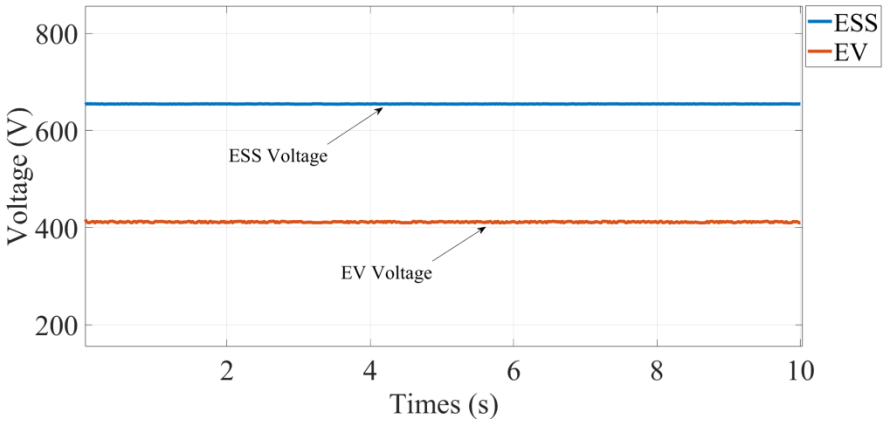

Figure 20. Battery Voltage vs Times (Mode 3)

CONCLUSION

The simulation results confirm that integrating a solar system and an ESS with EV charging infrastructure significantly enhances the utilization of renewable energy while reducing dependency on the conventional power grid. The study identifies optimal configurations of solar panels and ESS to efficiently meet EV charging demands. By implementing MPPT, PI control, and a bidirectional converter, the system achieves a well-regulated energy flow, ensuring stable charging and discharging operations. The results demonstrate that the bidirectional converter operates effectively in both buck and boost modes, achieving efficiencies of 95.3% and 94.8%, respectively, with power transfer rates of 20 kW and 22 kW. Additionally, solar irradiance of 1000 W/m² and a temperature of 10 °C were found to provide the highest charging efficiency, allowing the ESS to reach full charge in approximately 1.2 hours. These findings emphasize the potential of integrating renewable energy with smart control strategies to create sustainable EV charging stations that reduce grid reliance, improve energy efficiency, and support the transition toward a cleaner transportation ecosystem.

When benchmarked against existing commercial charging systems, the proposed solution offers competitive performance. While standard Level 2 AC chargers typically deliver 7 – 11 kW with efficiencies around 90 – 92% and require 4 – 8 hours for a full charge, the presented system achieves significantly faster charging with higher energy conversion efficiency, comparable to mid-tier DC fast chargers. This highlights the system's suitability for efficient and sustainable EV charging, especially in renewable-powered or off-grid contexts.

Additionally, this study provides a foundation for future advancements such as implementing real-time control mechanisms for adaptive energy management, enabling V2G functionality to support grid services, and integrating grid-interactive behavior for peak load shaving or demand response applications. These developments would enhance system responsiveness, promote grid stability, and transform EV charging stations into active components of a smart, renewable-powered energy infrastructure.

ACKNOWLEDGMENT

The authors would like to express sincere gratitude to the individuals and organizations who have contributed to this research project. First, the authors would like to thank Petronas Research Sdn. Bhd. for their support. The authors would also like to thank the CHAdeMO Association for their continuous technical support. Finally, the authors would like to thank the College of Engineering, Universiti Teknologi MARA for the excellent facility provided for the research, administrative support, and technical assistance.

NOMENCLATURE

A	current	[A]
V	voltage	[V]
P	power	[W]
SOC	state of charge	[%]

Abbreviations

AC	Alternating Current
BDC	Bidirectional DC-DC Converter
BEV	Battery Electric Vehicle
DC	Direct Current
EVSE	Electric Vehicle Supply Equipment
ESS	Energy Storage System
EV	Electric Vehicle
MPPT	Maximum Power Point Tracking
PI	Proportional Integral

REFERENCES

1. E. Sortomme and M. A. El-Sharkawi, "Optimal scheduling of vehicle-to-grid energy and ancillary services," *IEEE Trans Smart Grid*, vol. 3, no. 1, pp. 351–359, Mar. 2012, https://doi.org/10.1109/TSG.2011.2164099.
2. M. A. A. Hassan, E. Abdullah, N. H. N. Ali, N. M. Hidayat, M. Umair, and A. R. bin Johari, "Vehicle-to-grid system optimization for electric vehicle - a review," in *IOP Conference Series: Earth and Environmental Science*, Institute of Physics, 2023. https://doi.org/10.1088/1755-1315/1281/1/012076.
3. R. Menges and F. Eckenfels, "Integrating Energy and Water Management in a Low Mountain Region: A Project for Coupled Ecosystem Services," *Journal of Sustainable Development of Energy,* Water *and Environment Systems*, vol. 12, no. 4, pp. 1–22, Dec. 2024, https://doi.org/10.13044/j.sdewes.d12.0521.
4. F. N. Esfahani, A. Darwish, and B. W. Williams, "Power Converter Topologies for Grid-Tied Solar Photovoltaic (PV) Powered Electric Vehicles (EVs)—A Comprehensive Review," Jul. 01, 2022, *MDPI*. https://doi.org/10.3390/en15134648.
5. M. A. Hannan, M. M. Hoque, S. E. Peng, and M. N. Uddin, "Lithium-Ion Battery Charge Equalization Algorithm for Electric Vehicle Applications," *IEEE Trans Ind Appl*, vol. 53, no. 3, pp. 2541–2549, May 2017, https://doi.org/10.1109/TIA.2017.2672674.
6. F. N. Esfahani, A. Darwish, and B. W. Williams, "Power Converter Topologies for Grid-Tied Solar Photovoltaic (PV) Powered Electric Vehicles (EVs)—A Comprehensive Review," *Energies 2022, Vol. 15, Page 4648*, vol. 15, no. 13, p. 4648, Jun. 2022, https://doi.org/10.3390/EN15134648.
7. A. Kalair, N. Abas, M. S. Saleem, A. R. Kalair, and N. Khan, "Role of energy storage systems in energy transition from fossil fuels to renewables," *Energy Storage*, vol. 3, no. 1, Feb. 2021, https://doi.org/10.1002/est2.135.
8. Y. Zhou, M. Wang, H. Hao, L. Johnson, H. Wang, and H. Hao, "Plug-in electric vehicle market penetration and incentives: a global review," *Mitig Adapt Strateg Glob Chang*, vol. 20, no. 5, pp. 777–795, Jun. 2015, https://doi.org/10.1007/S11027-014-9611-2/METRICS.
9. C. Bhardwaj, J. Axsen, and D. McCollum, "Simulating automakers' response to zero emissions vehicle regulation," *Transp Res D Transp Environ*, vol. 94, p. 102789, May 2021, https://doi.org/10.1016/J.TRD.2021.102789.
10. J. A. Sanguesa, V. Torres-Sanz, P. Garrido, F. J. Martinez, and J. M. Marquez-Barja, "A review on electric vehicles: Technologies and challenges," Mar. 01, 2021, *MDPI*. https://doi.org/10.3390/smartcities4010022.
11. M. A. Yasko, "Analysis, Design and Simulation of Buck Converter for Photovoltaic System," in *2018 22nd International Conference Electronics, ELECTRONICS 2018*, Institute of Electrical and Electronics Engineers Inc., Aug. 2018. https://doi.org/10.1109/ELECTRONICS.2018.8443646.
12. D. C. Erb, O. C. Onar, and A. Khaligh, "Bi-directional charging topologies for plug-in hybrid electric vehicles," in *Proc. 25th Annu. IEEE Appl. Power Electron. Conf. Expo. (APEC),* Palm Springs, CA, USA, Feb. 2010, pp. 2066–2072.
13. A. Khan, S. Memon, and T. P. Sattar, "Integration and management of solar energy for electric vehicle charging station," in Solar World Congress 2017 - Innovation for the 100% Renewable Energy Transformation, Abu Dhabi, UAE, Nov. 2017, https://doi.org/10.18086/swc.2017.16.03.
14. M. Umair, N. M. Hidayat, A. Sukri Ahmad, N. H. Nik Ali, M. I. M. Mawardi, and E. Abdullah, "A renewable approach to electric vehicle charging through solar energy storage," *PLoS One*, vol. 19, no. 2, p. e0297376, Feb. 2024, https://doi.org/10.1371/JOURNAL.PONE.0297376.

15. M. Berrehil El Kattel, R. Mayer, F. Ely, and B. de Jesus Cardoso Filho, "Comprehensive review of battery charger structures of EVs and HEVs for levels 1–3," *International Journal of Circuit Theory and Applications*, vol. 51, no. 7, pp. 3514–3542, Jul. 2023, https://doi.org/10.1002/CTA.3579.
16. J. A. Sanguesa, V. Torres-Sanz, P. Garrido, F. J. Martinez, and J. M. Marquez-Barja, "A review on electric vehicles: Technologies and challenges," *Smart Cities*, vol. 4, no. 1, pp. 372–404, Mar. 2021, https://doi.org/10.3390/SMARTCITIES4010022.
17. M. A. Yasko, "Analysis, Design and Simulation of Buck Converter for Photovoltaic System," *2018 22nd International Conference Electronics, ELECTRONICS 2018*, Aug. 2018, https://doi.org/10.1109/ELECTRONICS.2018.8443646.
18. S. Jaman, B. Verbrugge, A. Zhaksylyk, T. Geury, M. El Baghdadi, and O. Hegazy, "Development of Smart Charging Scheduling and Power Management Strategy of a PV-ESS based Scalable EV Charging Station," *Transportation Research Procedia*, vol. 72, pp. 1240–1247, Jan. 2023, https://doi.org/10.1016/J.TRPRO.2023.11.583.
19. H. M. Abdullah, A. Gastli, and L. Ben-Brahim, "Reinforcement Learning Based EV Charging Management Systems-A Review," *IEEE Access*, vol. 9, pp. 41506–41531, 2021, https://doi.org/10.1109/ACCESS.2021.3064354.
20. P. Alaee, J. Bems, and A. Anvari-Moghaddam, "A Review of the Latest Trends in Technical and Economic Aspects of EV Charging Management," *Energies 2023, Vol. 16, Page 3669*, vol. 16, no. 9, p. 3669, Apr. 2023, https://doi.org/10.3390/EN16093669.
21. X. Gong and J. Rangaraju, Taking Charge of Electric Vehicles—Both in the Vehicle and on the Grid. Technical Report, Texas Instruments. Dallas, Texas, USA, 2018.
22. Integration and Management of Solar Energy for Electric Vehicle Charging Station - University of Huddersfield Research Portal, https://pure.hud.ac.uk/en/publications/integration-and-management-of-solar-energy-for-electric-vehicle-c, [Accessed: Sep. 10, 2025].
23. H. Ramakrishnan and J. Rangaraju, Power Topology Considerations for Electric Vehicle Charging Stations. Application Report, Texas Instruments. Dallas, Texas, USA, 2020.
24. M. I. M. Mawardi, N. H. N. Ali, N. M. Hidayat, E. Abdullah, M. Umair, and A. S. Ahmad, "Simulation Study of Power Transfer Efficiency in Non-Isolated Buck-Boost Bidirectional Converter for Electric Vehicle," in *2024 IEEE Sustainable Power and Energy Conference (iSPEC)*, IEEE, Nov. 2024, pp. 512–517. https://doi.org/10.1109/iSPEC59716.2024.10892389.
25. M. Umair, N. M. Hidayat, N. H. N. Ali, E. Abdullah, A. R. Bin Johari, and T. Hakomori, "The effect of vehicle-to-grid integration on power grid stability: A review," *IOP Conf Ser Earth Environ Sci*, vol. 1281, no. 1, p. 012070, Dec. 2023, https://doi.org/10.1088/1755-1315/1281/1/012070.
26. M. Umair, N. M. Hidayat, A. Sukri Ahmad, N. H. Nik Ali, M. I. M. Mawardi, and E. Abdullah, "A renewable approach to electric vehicle charging through solar energy storage," *PLoS One*, vol. 19, no. 2 February, Feb. 2024, https://doi.org/10.1371/journal.pone.0297376.
27. Syafii, Krismadinata, Muladi, T. K. Agung, and D. A. Sandri, "Simple Photovoltaic Electric Vehicles Charging Management System Considering Sun Availability Time," *Journal of Sustainable Development of Energy, Water and Environment Systems*, vol. 12, no. 1, Mar. 2024, https://doi.org/10.13044/J.SDEWES.D11.0476.
28. R. Ghotge, A. van Wijk, and Z. Lukszo, "Off-grid solar charging of electric vehicles at long-term parking locations," *Energy*, vol. 227, p. 120356, Jul. 2021, https://doi.org/10.1016/J.ENERGY.2021.120356.
29. G. R. Chandra Mouli, P. Bauer, and M. Zeman, "System design for a solar powered electric vehicle charging station for workplaces," *Appl Energy*, vol. 168, pp. 434–443, Apr. 2016, https://doi.org/10.1016/j.apenergy.2016.01.110.

30. M. A. N. Zelan *et al.*, "A simulation-based investigation into the charging performance of lithium-ion and lead-acid batteries in electric vehicles," in *IOP Conference Series: Earth and Environmental Science*, Institute of Physics, 2023. https://doi.org/10.1088/1755-1315/1281/1/012068.
31. M. Umair, N. M. Hidayat, N. H. N. Ali, E. Abdullah, A. R. bin Johari, and T. Hakomori, "The effect of vehicle-to-grid integration on power grid stability: A review," in *IOP Conference Series: Earth and Environmental Science*, Institute of Physics, 2023. https://doi.org/10.1088/1755-1315/1281/1/012070.
32. M. Awad, A. M. Ibrahim, Z. M. Alaas, A. El-Shahat, and A. I. Omar, "Design and analysis of an efficient photovoltaic energy-powered electric vehicle charging station using perturb and observe MPPT algorithm," *Front Energy Res*, vol. 10, Aug. 2022, https://doi.org/10.3389/fenrg.2022.969482.
33. B. Xu, A. A. Heidari, F. Kuang, S. Zhang, H. Chen, and Z. Cai, "Performance optimization of photovoltaic systems: Reassessment of political optimization with a quantum Nelder-mead functionality," *Solar Energy*, vol. 234, pp. 39–63, Mar. 2022, https://doi.org/10.1016/J.SOLENER.2022.01.048.
34. A. H. Almarzoogee and A. H. Mohammed, "Design a Bidirectional DC/DC Converter for Second-Level Electric Vehicle Bidirectional Charger," in *4th International Symposium on Multidisciplinary Studies and Innovative Technologies, ISMSIT 2020 - Proceedings*, Institute of Electrical and Electronics Engineers Inc., Oct. 2020. https://doi.org/10.1109/ISMSIT50672.2020.9254306.
35. A. K. Jaiswal, A. K. Panda, L. Senapati, S. K. Behera, and S. Behera, "Design of a Level-3 DC Fast Charging Station for EVs Using a Dual Active Bridge DC-DC Converter," in *IECON Proceedings (Industrial Electronics Conference)*, IEEE Computer Society, 2023. https://doi.org/10.1109/IECON51785.2023.10312734.

Paper submitted: 10.03.2025
Paper revised: 04.10.2025
Paper accepted: 09.10.2025